

# Molecular evaluation of thrombosis using X-ray phase contrast imaging with microbubbles targeted to P-selectin in mice

Rongbiao Tang<sup>1</sup> · Wei-Min Chai<sup>1</sup> · Fuhua Yan<sup>1</sup> · Guo-Yuan Yang<sup>2</sup> · Ke-Min Chen<sup>1</sup>

Received: 25 May 2015 / Revised: 15 November 2015 / Accepted: 19 November 2015 / Published online: 2 December 2015  
© European Society of Radiology 2015

## Abstract

**Objectives** X-ray phase contrast imaging (PCI) provides excellent image contrast by utilizing the phase shift. The introduction of microbubbles into tissues can cause a phase shift to make microbubbles visibly identified on PCI. In this study, we assessed the feasibility of targeted microbubble-based PCI for the detection of thrombosis.

**Methods** The absorption and phase contrast images of P-selectin-targeted microbubbles (MB<sub>P</sub>) were obtained and compared in vitro. MB<sub>B</sub>, control IgG-targeted microbubbles (MB<sub>C</sub>), and unbound microbubbles (MB<sub>U</sub>) were tested for binding specificity on thrombi expressing P-selectin. MB<sub>P</sub> were used as molecular PCI probes to evaluate P-selectin expression in a mouse model of arteriovenous shunt thrombosis that was created using PE tubes in the bypass outside of the mouse body.

**Results** PCI clearly showed the microbubbles not viewable via absorption contrast imaging (ACI). In vitro attachment of MB<sub>P</sub> (91.60±11.63) to thrombi was significantly higher than attachment of MB<sub>C</sub> (17.80±4.02,  $P<0.001$ ) or MB<sub>U</sub>

(9.80±2.59,  $P<0.001$ ). In the mouse model of arteriovenous shunt thrombosis, the binding affinity of MB<sub>P</sub> (15.50±6.25) was significantly greater than that of MB<sub>C</sub> (0.50±0.84,  $P<0.001$ ) or MB<sub>U</sub> (0.33±0.52,  $P<0.001$ ).

**Conclusions** Our results indicate that molecular PCI may be considered as a novel and promising imaging modality for the investigation of thrombosis.

## Key Points

- Small thrombi are rarely detected by conventional radiography.
- Phase contrast imaging (PCI) provides higher contrast and spatial resolution than conventional radiography.
- P-selectin targeted microbubbles detected by PCI may suggest early thrombosis.

**Keywords** Synchrotron radiation · Phase contrast imaging · Thrombosis · P-selectin · Microbubbles

## Introduction

Thrombosis is a major cause of morbidity and mortality worldwide [1]. Currently available imaging modalities for the detection of thrombosis mainly include optical imaging, PET, ultrasound imaging (USI), MRI, and CT [2–10]. However, such imaging methods have difficulty detecting early thrombosis, which always presents with a relatively small thrombus. Therefore, more sensitive imaging approaches are required. Molecular imaging is an emerging field that encompasses various advanced imaging techniques using cellular and molecular biology [11–14]. Molecular imaging relies on the administration of exogenously added probes to detect and quantitatively measure the desired cellular or molecular processes in vitro and in vivo [15–18]. Microbubbles targeted to adhesion molecules, such as P-selectin, VCAM-1, and

**Electronic supplementary material** The online version of this article (doi:10.1007/s00330-015-4129-x) contains supplementary material, which is available to authorized users.

✉ Rongbiao Tang  
tangme8688258@sina.com

✉ Ke-Min Chen  
keminchenrj@163.com

<sup>1</sup> Department of Radiology, Shanghai Jiao Tong University School of Medicine, Rui Jin Hospital, Shanghai 200025, People's Republic of China

<sup>2</sup> Neuroscience and Neuroengineering Center, Med-X Research Institute, Shanghai Jiao Tong University, Shanghai 200030, People's Republic of China

glycoprotein IIb/IIIa, have been shown to allow for real-time molecular USI of early thrombosis [13, 19, 20]. However, USI is easily disturbed by gas; therefore, USI is not an ideal imaging technique for gas-filled organs.

Conventional absorption contrast imaging (ACI) creates contrast relying on X-ray attenuation by an object. The weakly absorbing tissues are often not clearly shown by ACI. In addition to absorption, phase shift is another contrast mechanism between X-rays and tissue. By using the phase shift, phase contrast imaging (PCI) can afford more detailed images of soft tissues [21–29]. Synchrotron radiation (SR) imaging can visibly show the microvasculature due to its high resolution [30, 31]. SR-based PCI has been used for clinical mammography with its high sensitivity to soft tissues [32]. PCI has high penetration power for deep tissue detection. In addition, PCI is not disturbed by gas; therefore, PCI can be used to visualize gas-filled organs, such as lung and abdomen. Microbubbles are currently used as USI contrast agents. Moreover, microbubbles can be considered suitable contrast agents for PCI [27, 33]. Because gas has a different refractive index from that of the surrounding tissues, the gas–tissue interfaces can generate significant phase shifts that make the boundaries highly visible on PCI [29, 33, 34]. Various molecular probes (such as proteins, peptides, and antibodies) can be attached to the shell surface of microbubbles. The values of the above-mentioned applications suggest the potential for PCI to clearly show targeted microbubbles to evaluate the expression of biological targets.

In the present work, we established a mouse model of arteriovenous shunt thrombosis and imaged P-selectin expression using high-resolution PCI with microbubbles targeted to P-selectin.

## Material and methods

### Antibody-microbubble conjugation

Streptavidin-bound microbubbles (Targestar-SA) were obtained from Targeson (San Diego, CA, USA). The size distribution of the microbubbles was determined using a Coulter counter (AccuSizer, Santa Barbara, CA, USA). Biotinylated mouse P-selectin (553743; BD Pharmingen) and an isotype control rat IgG antibody (R3-34; BD Pharmingen) were obtained. The microbubbles were conjugated to the antibodies using a biotin-streptavidin interaction. Briefly, the Targestar-SA microbubble solution was centrifuged (400 g for 4 min) to separate the microbubbles from the liquid, and then the liquid was discarded. According to the manufacturer's instructions, one vial of Targestar-SA can couple with approximately 100 µg of biotinylated IgG antibodies. The microbubbles were incubated with 200 µg of the respective antibodies at room temperature for 20 min. This incubation resulted in an

excess of biotinylated IgG antibodies to achieve the goal of saturation all of the streptavidin binding sites on the microbubbles. The purification of conjugated microbubbles was performed via three centrifuge washes (400 g for 4 min) to remove the unbound antibodies. The conjugated microbubble concentration was determined using a Neubauer haemocytometer.

### Microbubble immunofluorescence staining

FITC-labelled goat anti-rat secondary antibody (Santa Cruz Biotechnology) was used to confirm the presence of primary antibodies on the surfaces of the bound microbubbles. P-selectin-targeted microbubbles (MB<sub>P</sub>) or control IgG-targeted microbubbles (MB<sub>C</sub>) were incubated with the secondary antibody in a 1:200 ratio at room temperature for 1 h and washed with physiological saline. Unbound microbubbles (MB<sub>U</sub>) treated with only secondary antibody were used as a control. Microbubbles were placed on glass coverslips and observed under a Leica DM2500 microscope.

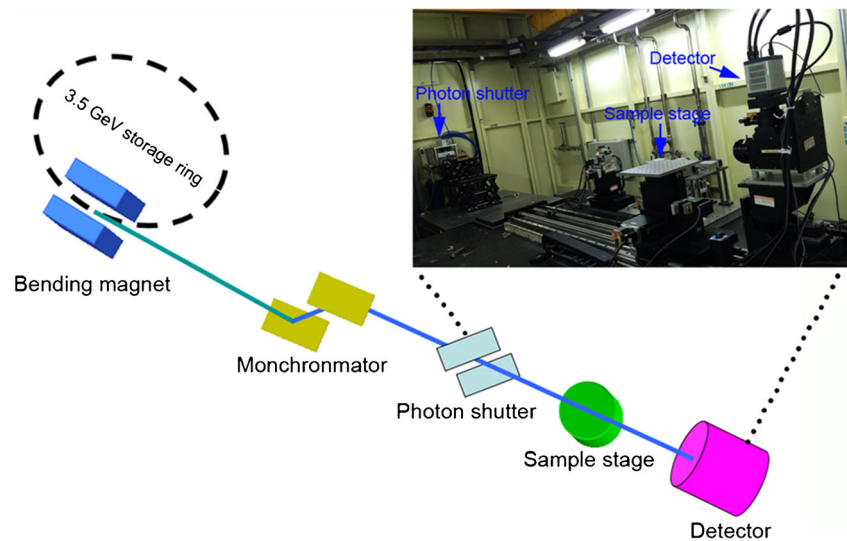
### SR parameters

Images were acquired at the BL13W1 beamline at the Shanghai Synchrotron Radiation Facility (SSRF) in China. X-rays were generated using a 3.5 GeV electron storage ring and were monochromatized using a double-crystal monochromator with Si(111) and Si(311) crystals. The energy of the beamline could be varied from 8 to 72.5 keV. The energy resolution ( $\Delta E/E$ ) was less than  $5 \times 10^{-3}$ . The transmitted X-rays were captured by a 100-µm-thick CdWO<sub>4</sub> cleaved single-crystal scintillator and converted to a visible image. A high-precision sample stage that allowed for the positioning of a sample in all six axes was placed 34 m downstream of the synchrotron source. The distance between the sample stage and photon shutter was 1.7 m. The sample-to-detector distance (SDD) was changeable with a range of 8 m (Fig. 1).

### Comparison between ACI and PCI

Microbubbles were placed in a PE-50 catheter that was set perpendicular to the X-ray beam. According to the imaging principles of in-line PCI, phase and absorption contrast information can be selected by changing the SDD [26, 27]. ACI can be performed with the SDD of near 0. Therefore, the SDDs for ACI and PCI were set to 5 mm and 30 cm, respectively. With the exception of SDD, all the other imaging parameters for ACI and PCI were the same. The distance was changed by moving the CCD camera on a rail. The relative densities were assessed via line profile analysis using Image-Pro Plus 6.0.

**Fig. 1** Schematic of the in-line PCI setup at the BL13W1 in SSRF. The distance between the radiation source and sample stage was 34 m. The inset picture shows the distance between the photon shutter and sample stage of 1.7 m. The SDD was adjustable from 0 to 8 m by moving the detector on the rail



### The arteriovenous shunt thrombosis model and imaging

All experiments were performed in accordance with the guidelines for the care and use of laboratory animals of Shanghai Jiao Tong University. Eighteen male C57BL/6 mice at 6 to 7 weeks of age (weighing 20 to 25 grams) were obtained from the Animal Center, CAS, Shanghai, China, and kept under pathogen-free conditions. The mice were anaesthetized before the surgical procedure via an intraperitoneal injection of ketamine ( $100 \text{ mg kg}^{-1}$ ) and xylazine ( $10 \text{ mg kg}^{-1}$ ). A midline incision on the neck was made under an operating microscope. The right carotid artery and left jugular vein were exposed. Two 20-cm-long PE-10 catheters connected with a 20-cm-long PE-50 catheter were used to assemble the arteriovenous shunt vessel (Fig. 2). The proximal end of an 8-mm-long silk thread was fixed in the middle of the PE-50 catheter using 502 super glue. An 8-cm-long PE-10 catheter was connected to the PE-50 catheter up to the location of the silk thread. The whole shunt vessel was filled with physiological saline without any air bubbles. One terminus of the shunt vessel was cannulated into the right carotid artery. Next,  $150 \mu\text{L}$  of heparin ( $75 \text{ U/mL}$ ) was injected into the right carotid artery through the other terminus of the shunt vessel that was connected to a 1-mL syringe (BD). A microvascular clip was then used to temporally clamp the right carotid artery. The 1-mL syringe was removed, and the terminus of the shunt vessel was cannulated into the left jugular vein. Subsequently, the microvascular clip was removed to create arterial and venous bypasses for the blood to flow. After 25 min of blood circulation,  $1 \times 10^7$   $\text{MB}_P$ ,  $\text{MB}_C$ , or  $\text{MB}_U$  were injected into the shunt vessel through the 8-cm-long PE-10 catheter attached to a 1-mL BD syringe (injection time, 4 s). The PE-50 catheter was placed such that the silk thread was

perpendicular to the X-ray beam. Imaging of the retained microbubbles was performed 10 min after the injection. The numbers of  $\text{MB}_P$ ,  $\text{MB}_C$ , and  $\text{MB}_U$  adhered onto the silk thread were calculated from the 18 mice (three groups of six mice in each group).

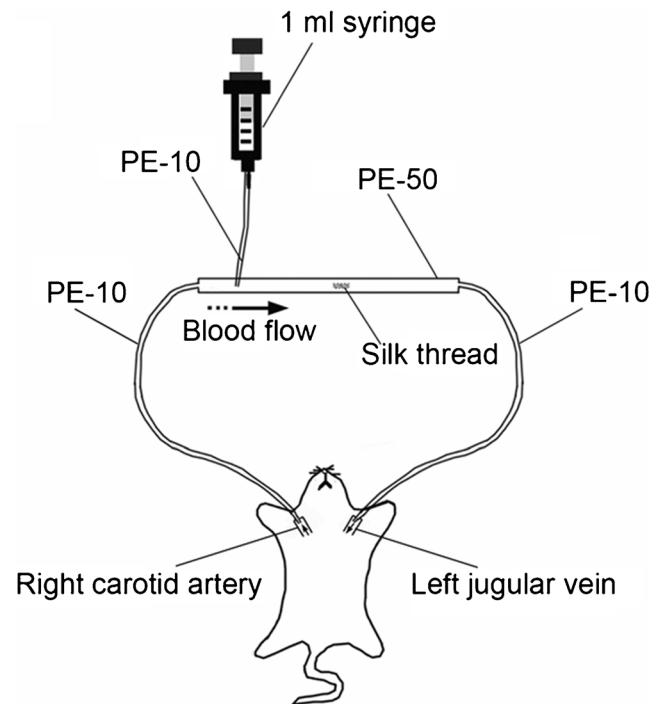
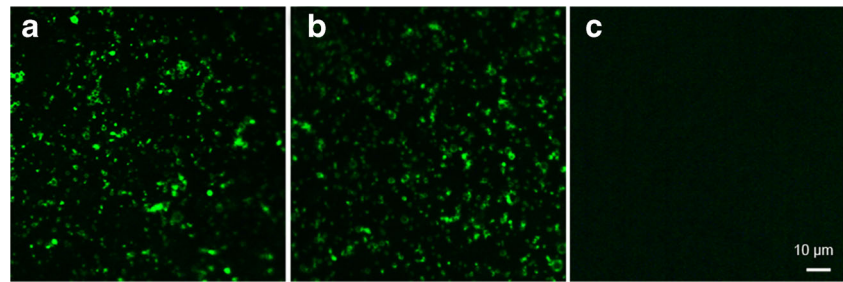


**Fig. 2** Schematic of the method for the arteriovenous shunt thrombosis. The two termini of the PE-10 catheters were cannulated into the right carotid artery and left jugular vein, respectively. The length of the PE-10 catheter was 20 cm. The two PE-10 catheters were connected by a 20-cm-long PE-50 catheter. An 8-mm-long silk thread was fixed in the middle of the PE-50 catheter. The microbubbles were injected using a 1-mL syringe via a PE-10 catheter up to the location of the silk thread

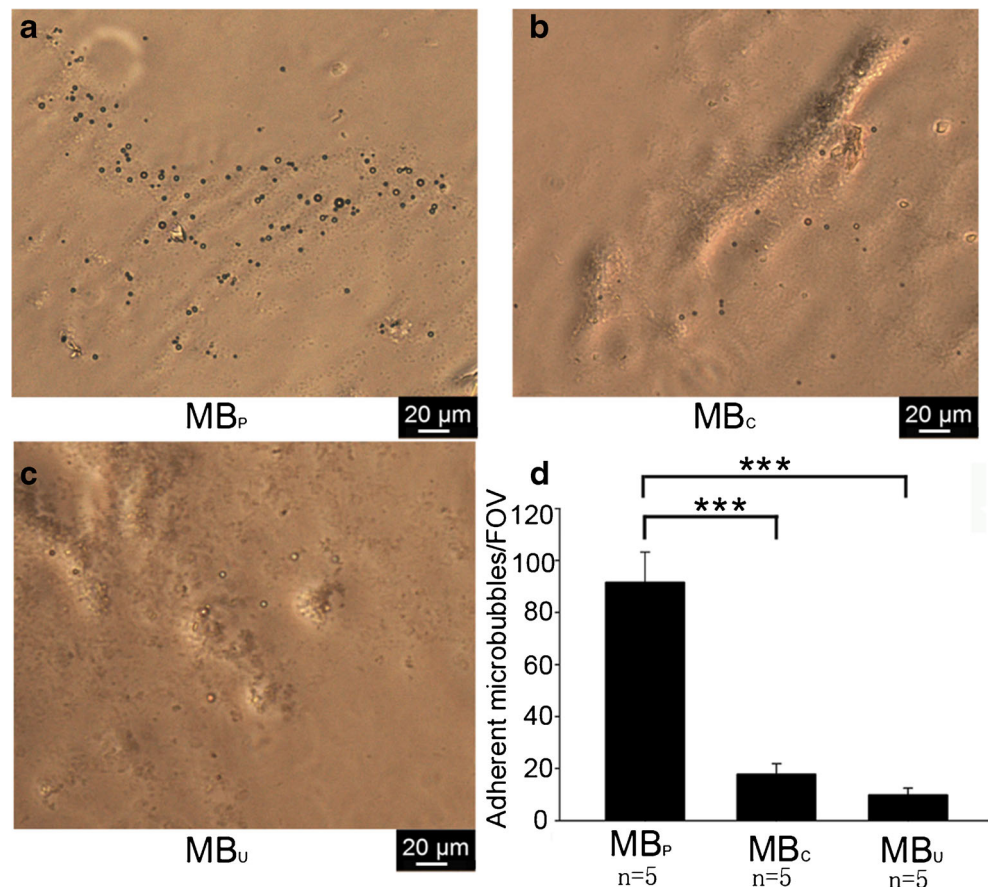
**Fig. 3** Fluorescence microscopy images of MB<sub>P</sub> (a), MB<sub>C</sub> (b), and MB<sub>U</sub> (c) stained with fluorescent secondary antibodies. Note the *bright green* fluorescence confirmed the presence of P-selectin (a) or control IgG antibodies (b) on microbubbles



### In vitro adhesion studies

After the thrombi were formed on the silk thread, they were daubed onto different coverslips. The coverslips were incubated with  $5 \times 10^6$  MB<sub>P</sub>, MB<sub>C</sub>, or MB<sub>U</sub>. Owing to the buoyancy of the microbubbles, the coverslips were inverted to maximize the exposure of the thrombi to the microbubbles. After a 3-min static exposure, the coverslips were gently washed in physiological saline to remove the unbound microbubbles. The number of attached microbubbles was determined under a Leica optical microscope in five randomly selected fields of view (FOV). Images were obtained using a Leica Application Suite software platform. The area of the thrombi on the coverslip was at least 20 times larger than that of the FOV, so the randomly selected five FOVs were non-overlapping.

**Fig. 4** In vitro adhesion of the microbubbles to the thrombi. Representative optical microscopic images of adhesion assays demonstrating that more MB<sub>P</sub> (a) attached to the thrombi than MB<sub>C</sub> (b) and MB<sub>U</sub> (c). **d** Quantitative assay of the number of microbubbles attached to the thrombi in five randomly selected FOV. FOV=0.1 mm<sup>2</sup>. \*\*\* $P < 0.001$ . (Original magnification,  $\times 200$ )



### Thrombi immunohistochemistry

Immunostaining for P-selectin was performed on paraffin-embedded sections of thrombus tissue. Briefly, heat-induced epitope retrieval was performed using a pressure cooker with sodium citrate buffer. The sections were rinsed with PBS for 5 min and blocked with 5 % bovine serum albumin (BSA) for 30 min at 37 °C. The tissues were incubated using a rabbit anti mouse-CD62P primary antibody (Abcam) for 12 h at 4 °C and then incubated with an HRP-conjugated goat anti-rabbit secondary antibody (Abcam) for 1 h at room temperature. Control staining was performed using only the HRP-conjugated secondary antibody. The slides were counterstained for 5 min in haematoxylin, dehydrated, mounted, and photographed on a Leica light microscope.

## Statistical analysis

The statistical package GraphPad InStat 3 was used for all analyses. The data were presented as the means±the standard deviations (SDs). Data were analysed using one-way analysis of variance (ANOVA) followed by Bonferroni test. The differences were considered statistically significant at  $P<0.05$ .

## Results

### Conjugation of the antibodies to the microbubbles and in vitro binding experiments

FITC-labelled secondary antibody was used as a probe to confirm the conjugation of P-selectin or control IgG antibodies to the microbubbles. MB<sub>P</sub> or MB<sub>C</sub> exhibited green spherical shapes after they were incubated with the green fluorescent secondary antibody (Fig. 3a, b). As shown in Fig. 3c, no evident binding-dependent fluorescence was observed on the surface of MB<sub>U</sub>. The mean diameter size of MB<sub>P</sub> was  $1.94\pm 5.99\ \mu\text{m}$  (Supplementary Fig. 1). After a 3-min static exposure to the thrombi, the attachment of MB<sub>P</sub> was significantly greater than that of either MB<sub>C</sub> or MB<sub>U</sub> ( $91.60\pm 11.63$  versus  $17.80\pm 4.02$  versus  $9.80\pm 2.59$ , respectively;  $P<0.001$ ; Fig. 4).

### SR imaging of the microbubbles

To illustrate the advantage of PCI for imaging the microbubbles, PCI was compared with ACI. ACI and PCI were performed at an energy level of 19 keV but with two different SDDs ( $d=5\ \text{mm}$  and  $30\ \text{cm}$ , respectively). Because the density of the microbubbles was lower than that of the physiological saline, the microbubbles floated and assembled along the upper edge of the PE-50 catheter. Fig. 5a displays an MB<sub>P</sub> image taken at 5 mm. No distinct contrast between MB<sub>P</sub> and physiological saline can be detected. In comparison, PCI offered clear visualization of MB<sub>P</sub> (Fig. 5c). MB<sub>P</sub> caused a more visible change in intensity around the edges on PCI than on ACI (Fig. 5b, d). The image's clarity was determined by the resolution of the CCD. MB<sub>P</sub> were more clearly revealed by the CCD with a resolution of 325 nm than the CCD with a resolution of  $3.25\ \mu\text{m}$  (Supplementary Fig. 2). On PCI, the microbubbles created a phase shift variation that resulted in contrast changes around the edges of the microbubbles that appeared as light and dark fringes. The microbubbles appeared as white areas surrounded by annular black areas, which made them detectable (Supplementary Fig. 3a-c). Additionally, the microbubble diameter could be measured using line profile analysis (Image-Pro Plus 6.0), which identified both edges of a microbubble by

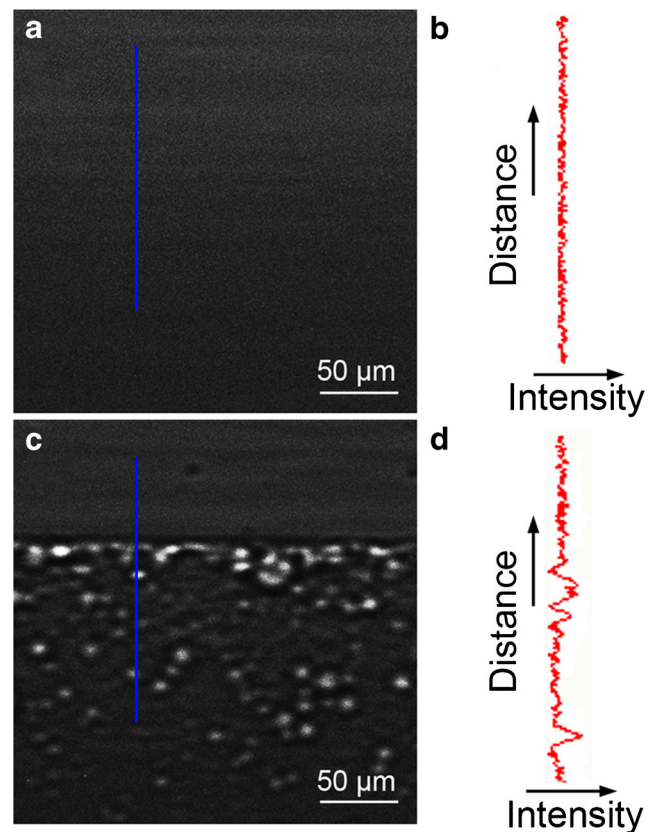


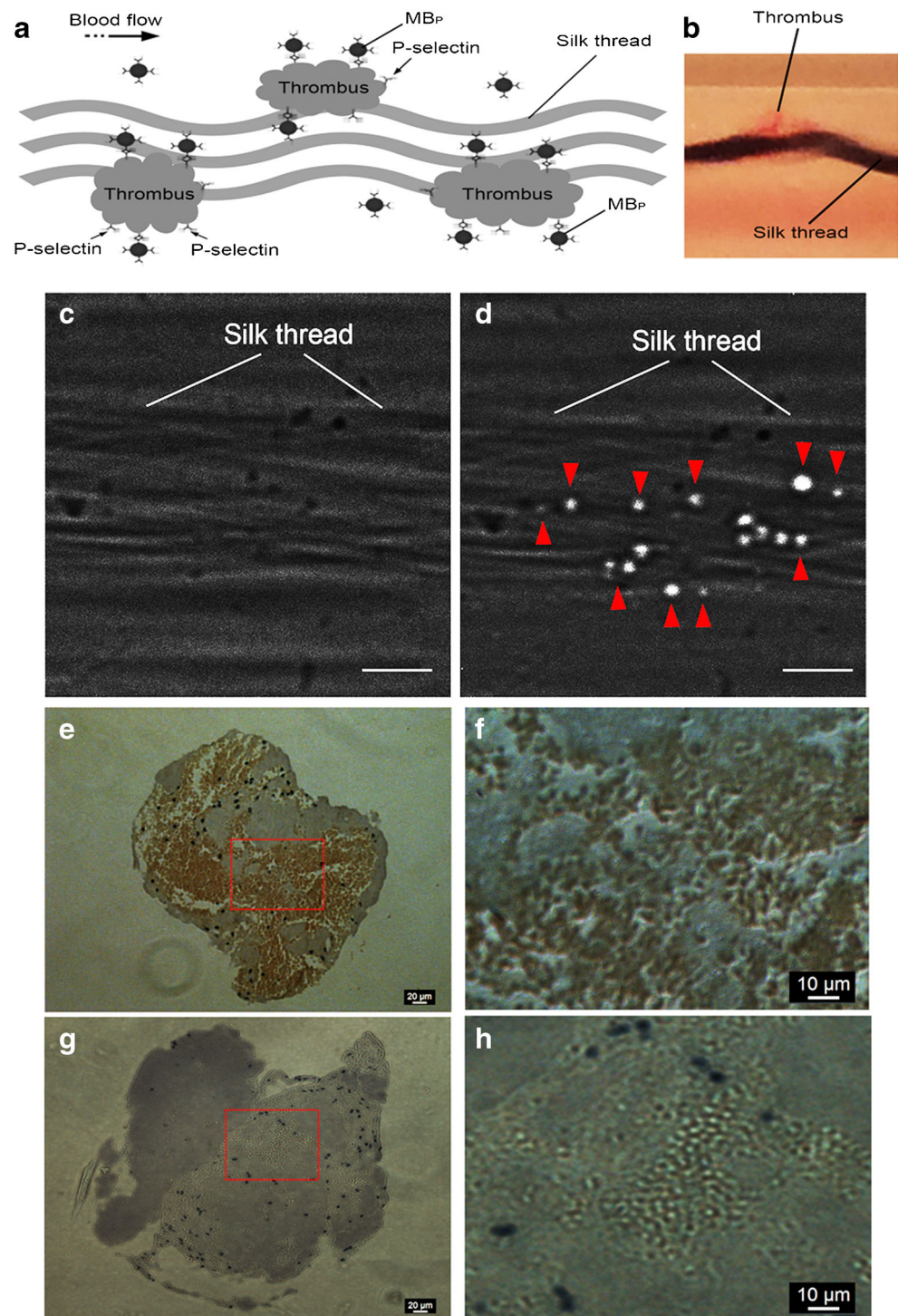
**Fig. 5** SR images of MB<sub>P</sub>. The microbubbles can clearly be seen on the phase contrast image (c), but not on the absorption contrast image (a). b and d are the line profile analyses of the intensity values along a straight line (blue) in (a) and (c), respectively. Note that the microbubbles caused a distinct change in intensity on the phase contrast image. The images were obtained at an energy of 19 keV with an SDD of 30 cm. The pixel size was  $325\ \text{nm}\times 325\ \text{nm}$ . The exposure time was 3 s

expressing a density variation curve (Supplementary Fig. 3d, e).

### PCI of P-selectin in the mouse model of arteriovenous shunt thrombosis

A mouse model of arteriovenous shunt thrombosis was successfully developed by assembling bypass blood flow between the right carotid artery and left jugular vein. The principles of the MB<sub>P</sub> attachment studies are described in Fig. 6a. After 25 min of blood circulation, some thrombi formed on the silk thread (Fig. 6b). MB<sub>P</sub> were found to specifically attach to the thrombi on the silk thread (Figs. 6d and 7a-c). P-selectin expression was confirmed on the thrombi by immunostaining (Fig. 6f, h). Few MB<sub>C</sub> or MB<sub>U</sub> were found to bind to the thrombi (Fig. 7d, e). Quantitative analysis revealed that the binding affinity of MB<sub>P</sub> was significantly greater than that of MB<sub>C</sub> or MB<sub>U</sub> ( $15.50\pm 6.25$  versus  $0.50\pm 0.84$  versus  $0.33\pm 0.52$ , respectively;  $P<0.001$ ; Fig. 7f).

**Fig. 6** PCI of microbubbles targeted to thrombi and immunohistochemical staining. **a** Schematic of  $MB_P$  binding to the thrombi.  $MB_P$  specifically bound to P-selectin expressed on the surface of the thrombi. Next,  $MB_P$  were imaged by PCI to evaluate P-selectin expression. **b** Some thrombi formed on the silk thread after 25 min of blood circulation. **c** Phase contrast image acquired before the injection of  $MB_P$ . **d** A phase contrast image acquired 10 min after the injection clearly showing that  $MB_P$  specifically attached to the thrombi. **f** and **h** are magnified images of the region in the red boxes in (e) and (g), respectively. The immunohistochemical analysis (f) indicated P-selectin expression (brown staining) on the thrombi. No brown staining (h) was observed on control staining. The phase contrast images were obtained at an energy of 19 keV with an SDD of 30 cm. The pixel size was  $325\text{ nm} \times 325\text{ nm}$ , and the exposure time was 3 s. Scale bars:  $50\text{ }\mu\text{m}$  (c, d)

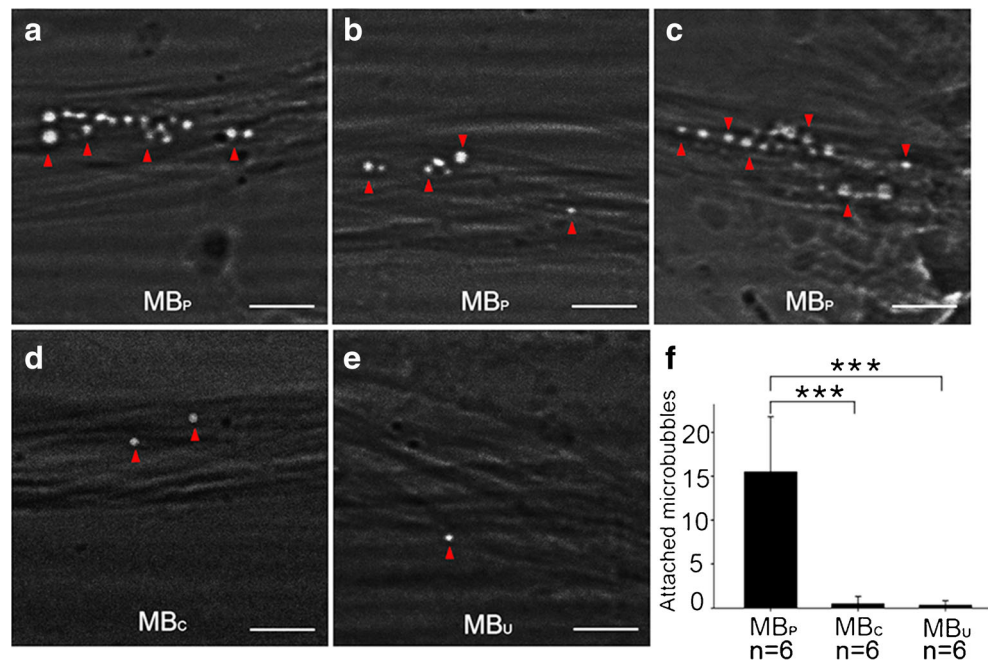


## Discussion

P-selectin is widely considered to be an important positive regulator during inflammatory responses [13, 17, 20, 35, 36]. The targeting of microbubbles to P-selectin has been found to greatly increase their retention within regions of thrombosis in previous studies [13, 19, 37, 38]. Microvascular retention of  $MB_P$  creates strong signal enhancement on USI of

inflammation and renal tissue injury [20]. Targeted contrast-enhanced USI enables noninvasive in vivo quantification and monitoring of P-selectin expression in inflammation in a murine model of chemically induced inflammatory bowel disease [39]. Similarly, we found that the binding affinity of  $MB_P$  was significantly greater than that of  $MB_C$  or  $MB_U$  in our mouse model of arteriovenous shunt thrombosis. The competitive binding experiments to confirm  $MB_P$ 's binding specificity

**Fig. 7** Representative phase contrast images of microbubbles attached to thrombi from five mice. PCI performed 10 minutes after microbubble injection visibly showed that more MB<sub>P</sub> (a–c) attached to the thrombi on the silk thread than MB<sub>C</sub> (d) or MB<sub>U</sub> (e). **f** Quantitative assay of the numbers of MB<sub>P</sub>, MB<sub>C</sub>, and MB<sub>U</sub> adhered to the silk thread (\*\**P*<0.001). The images were obtained at an energy of 19 keV with an SDD of 30 cm. The pixel size was 325 nm×325 nm, and the exposure time was 3 s. *Scale bars*: 50 μm



would be preferable over MB<sub>C</sub> or MB<sub>U</sub>, which may have different pharmacokinetic properties. However, the specific binding of antibody and antigen is still the most important factor affecting the binding characteristics. Using ultrasound molecular imaging (UMI), the abundant retention of these targeted microbubbles offers a strong ultrasound signal for the diagnosis of the early stages of thrombus formation [13, 20, 40]. UMI can visualize single microbubbles with picogram sensitivity [41]. However, microbubbles are required to oscillate to amplify the signal when they are used as an ultrasound contrast agent, but this is not needed in PCI [42]. By adding exposure time or X-ray energy, PCI has higher penetration power to show deep and heterogeneous as well as thick tissues.

Microbubbles have been effectively used as a contrast agent by analyser based imaging (ABI) [42–44] and X-ray dark-field imaging based on Talbot-Lau interferometry [45]. Both of these imaging modalities may be used to measure the concentration of microbubbles targeted towards biological markers. However, because the size of a microbubble is smaller than the detector pixel aperture, each single microbubble still cannot be detected independently [43]. Here, a single microbubble could be clearly shown using our in-line PCI system. This may allow the quantification of biological markers more precisely by counting the number of targeted microbubbles instead of measuring the concentration of targeted microbubbles. Because microbubbles generally contain gas and a biodegradable shell, these low-density materials absorb the synchrotron beam weakly, making microbubbles minimally identifiable with ACI. Instead, in-line PCI principally exploits phase shifts as the contrast mechanism. The gas core–tissue interface creates a significant phase shift to

enhance the image contrast, causing the microbubble to stand out from its surrounding tissues. Unbound microbubbles have been used as in-line PCI contrast agents to clearly visualize the architecture of the mouse renal vasculature, hepatic vessels and tumor-associated vessels [27, 33]. However, adhesion molecules expressed on vessels cannot be evaluated using these unbound microbubbles. By attaching various molecules to the shell surface of microbubbles, the targeted microbubbles can be used as molecular probes to evaluate the expression of biological targets. Based on its high spatial resolution and sensitivity for showing microbubbles, molecular PCI may be considered a promising imaging modality to estimate the binding affinities of bound microbubbles to their targets.

There are some limitations of the present study. The detector FOV is relatively small; further technical improvements are needed to enlarge the FOV for potential clinical applications. Additionally, the thrombosis was created using PE tubes in the bypass outside of the body rather than inside the body. MB<sub>P</sub> could be clearly detected by immobilizing the PE tubes, although the exposure time lasted up to 3 s. Motion image blurring may be found in a living mouse because the exposure time is too long. To prevent potential motion artefacts in vivo, sufficient temporal resolution is expected to shorten the exposure time. Further research is required to confirm whether similar findings can be obtained inside the bodies of living mice. We only obtained projection images in this study; the image contrast became weakened because of overlap of the projection. The diameter of the microbubble can be measured by using the intensity variation. However, the method is challenged when the concentration of the microbubbles is too high. The mean size of microbubbles is always determined

by measuring the diameters of a considerable number of microbubbles. However, some microbubbles cannot be detected clearly due to the overlap of the projection. In a further study, phase contrast CT may be used to avoid the overlap to measure the microbubbles more precisely.

## Conclusions

Our study shows that PCI allows the clear visualization of weakly absorbing microbubbles with high spatial resolution down to the submicron scale. Targeted contrast-enhanced PCI may enable quantification of P-selectin expression to suggest early thrombosis.

**Acknowledgments** The scientific guarantor of this publication is Rongbiao Tang. The authors of this manuscript declare no relationships with any companies, whose products or services may be related to the subject matter of the article. This study has received funding by the National Natural Science Foundation of China (Grant nos. 81301347, 81271740 and 81471808), Nation Basic Research Program of China (973 Program 2010CB834305), Shanghai Jiao Tong University Med-Science Cross Research Foundation (YG2013MS30), State Key Clinical Department of Medical Imaging and Shanghai College of first-class discipline. One of the authors has significant statistical expertise. Institutional Review Board approval was obtained. Approval from the institutional animal care committee was obtained. Methodology: prospective, experimental, performed at one institution.

## References

- Roger VL, Go AS, Lloyd-Jones DM et al (2011) Heart disease and stroke statistics—2011 update a report from the American Heart Association. *Circulation* 123:e18–e209
- Anderson CR, Hu X, Tlaxca J et al (2011) Ultrasound molecular imaging of tumor angiogenesis with an integrin targeted microbubble contrast agent. *Investig Radiol* 46:215
- Lee J-H, Huh Y-M, Y-w J et al (2007) Artificially engineered magnetic nanoparticles for ultra-sensitive molecular imaging. *Nat Med* 13:95–99
- Ntziachristos V, Tung C-H, Bremer C, Weissleder R (2002) Fluorescence molecular tomography resolves protease activity in vivo. *Nat Med* 8:757–761
- Phelps ME (2000) PET: the merging of biology and imaging into molecular imaging. *J Nucl Med* 41:661–681
- Popovtzer R, Agrawal A, Kotov NA et al (2008) Targeted gold nanoparticles enable molecular CT imaging of cancer. *Nano Lett* 8:4593–4596
- Sokolov K, Follen M, Aaron J et al (2003) Real-time vital optical imaging of precancer using anti-epidermal growth factor receptor antibodies conjugated to gold nanoparticles. *Cancer Res* 63:1999–2004
- Wang H, Zheng L, Peng C et al (2011) Computed tomography imaging of cancer cells using acetylated dendrimer-entrapped gold nanoparticles. *Biomaterials* 32:2979–2988
- Weissleder R, Moore A, Mahmood U et al (2000) In vivo magnetic resonance imaging of transgene expression. *Nat Med* 6:351–354
- Willmann JK, Paulmurugan R, Chen K et al (2008) US imaging of tumor angiogenesis with microbubbles targeted to vascular endothelial growth factor receptor type 2 in mice 1. *Radiology* 246:508–518
- Herschman HR (2003) Molecular imaging: looking at problems, seeing solutions. *Science* 302:605–608
- Massoud TF, Gambhir SS (2003) Molecular imaging in living subjects: seeing fundamental biological processes in a new light. *Genes Dev* 17:545–580
- Wang X, Hagemeyer CE, Hohmann JD et al (2012) Novel single-chain antibody-targeted microbubbles for molecular ultrasound imaging of thrombosis validation of a unique noninvasive method for rapid and sensitive detection of thrombi and monitoring of success or failure of thrombolysis in mice. *Circulation* 125:3117–3126
- Weissleder R, Pittet MJ (2008) Imaging in the era of molecular oncology. *Nature* 452:580–589
- Briley-Saebo KC, Mulder WJ, Mani V et al (2007) Magnetic resonance imaging of vulnerable atherosclerotic plaques: current imaging strategies and molecular imaging probes. *J Magn Reson Imaging* 26:460–479
- Thorek DL, Chen AK, Czupryna J, Tsourkas A (2006) Superparamagnetic iron oxide nanoparticle probes for molecular imaging. *Ann Biomed Eng* 34:23–38
- Warram JM, Sorace AG, Saini R, Umphrey HR, Zinn KR, Hoyt K (2011) A triple-targeted ultrasound contrast agent provides improved localization to tumor vasculature. *J Ultrasound Med* 30:921–931
- Weissleder R, Tung C-H, Mahmood U, Bogdanov A (1999) In vivo imaging of tumors with protease-activated near-infrared fluorescent probes. *Nat Biotechnol* 17:375–378
- Ferrante E, Pickard J, Rychak J, Klibanov A, Ley K (2009) Dual targeting improves microbubble contrast agent adhesion to VCAM-1 and P-selectin under flow. *J Control Release* 140:100–107
- Lindner JR, Song J, Christiansen J, Klibanov AL, Xu F, Ley K (2001) Ultrasound assessment of inflammation and renal tissue injury with microbubbles targeted to P-selectin. *Circulation* 104:2107–2112
- Tang R, Chai W-M, Yang G-Y, Xie H, Chen K-M (2012) X-ray phase contrast imaging of cell isolation with super-paramagnetic microbeads. *PLoS One* 7:e45597
- Meuli R, Hwu Y, Je JH, Margaritondo G (2004) Synchrotron radiation in radiology: radiology techniques based on synchrotron sources. *Eur Radiol* 14:1550–1560
- Sztrókay A, Herzen J, Auweter SD et al (2013) Assessment of grating-based X-ray phase-contrast CT for differentiation of invasive ductal carcinoma and ductal carcinoma in situ in an experimental ex vivo set-up. *Eur Radiol* 23:381–387
- Zhang X, Yang X-R, Chen Y et al (2013) Visualising liver fibrosis by phase-contrast X-ray imaging in common bile duct ligated mice. *Eur Radiol* 23:417–423
- Tang R, Yan F, Chai WM et al (2015) A novel imaging tool for hepatic portal system using phase contrast technique with hydrogen peroxide-generated O<sub>2</sub> gas. *J Synchrotron Radiat* 22:1263–1267
- Tang R, Chai W-M, Ying W et al (2012) Anti-VEGFR2-conjugated PLGA microspheres as an x-ray phase contrast agent for assessing the VEGFR2 expression. *Phys Med Biol* 57:3051
- Tang R, Xi Y, Chai W-M et al (2011) Microbubble-based synchrotron radiation phase contrast imaging: basic study and angiography applications. *Phys Med Biol* 56:3503
- Tang R, Huang W, Yan F et al (2013) In-line phase contrast imaging of hepatic portal vein embolization with radiolucent embolic agents in mice: a preliminary study. *PLoS One* 8, e80919
- Tang R, Li W-X, Huang W et al (2013) CO<sub>2</sub>-based in-line phase contrast imaging of small intestine in mice. *Scientific reports* 3
- Kobayashi S, Hori M, Dono K et al (2004) In vivo real-time microangiography of the liver in mice using synchrotron radiation. *J Hepatol* 40:405–408



31. Yuan F, Lin X, Guan Y et al (2014) Collateral circulation prevents masticatory muscle impairment in rat middle cerebral artery occlusion model. *J Synchrotron Radiat* 21:1314–1318
32. Castelli E, Tonutti M, Arfelli F et al (2011) Mammography with synchrotron radiation: first clinical experience with phase-detection technique. *Radiology* 259:684–694
33. Xi Y, Tang R, Wang Y, Zhao J (2011) Microbubbles as contrast agent for in-line x-ray phase-contrast imaging. *Appl Phys Lett* 99: 011101
34. Izadifar Z, Belev G, Izadifar M, Izadifar Z, Chapman D (2014) Visualization of ultrasound induced cavitation bubbles using the synchrotron x-ray analyzer based imaging technique. *Phys Med Biol* 59:7541
35. Falati S, Liu Q, Gross P et al (2003) Accumulation of tissue factor into developing thrombi in vivo is dependent upon microparticle P-selectin glycoprotein ligand 1 and platelet P-selectin. *J Exp Med* 197:1585–1598
36. Burger PC, Wagner DD (2003) Platelet P-selectin facilitates atherosclerotic lesion development. *Blood* 101:2661–2666
37. Takalkar AM, Klibanov AL, Rychak JJ, Lindner JR, Ley K (2004) Binding and detachment dynamics of microbubbles targeted to P-selectin under controlled shear flow. *J Control Release* 96:473–482
38. Rychak JJ, Lindner JR, Ley K, Klibanov AL (2006) Deformable gas-filled microbubbles targeted to P-selectin. *J Control Release* 114:288–299
39. Nirupama D, Lutz AM, Ying R et al (2012) Quantification and monitoring of inflammation in murine inflammatory bowel disease with targeted contrast enhanced. *Radiology* 262:172–180
40. Lindner JR, Dayton PA, Coggins MP et al (2000) Noninvasive imaging of inflammation by ultrasound detection of phagocytosed microbubbles. *Circulation* 102:531–538
41. Alexander LK, Peter TR, Michael SH et al (2004) Detection of individual microbubbles of ultrasound contrast agents: imaging of free-floating and targeted bubbles. *Investig Radiol* 39:187–195
42. Millard TP, Endrizzi M, Everdell N et al (2015) Evaluation of microbubble contrast agents for dynamic imaging with x-ray phase contrast. *Sci Rep* 5
43. Arfelli F, Rigon L, Menk RH (2010) Microbubbles as x-ray scattering contrast agents using analyzer-based imaging. *Phys Med Biol* 55:1643–1658(1616)
44. Millard TP, Endrizzi M, Rigon L et al (2013) Quantification of microbubble concentration through x-ray phase contrast imaging. *Appl Phys Lett* 103:114105 - 114105-114104
45. Velroyen A, Bech M, Malecki A et al (2013) Microbubbles as a scattering contrast agent for grating-based x-ray dark-field imaging. *Phys Med Biol* 58:N37–N46(10)